Field observations of aerosol physical and chemical properties in the Netherlands

Liu, Xinya

DOI:
10.33612/diss.1144463961

Chapter 1 Introduction

1.1 Atmospheric aerosol and its impact

Atmospheric aerosols are solid or liquid particles suspended in the air (Hinds and Zhu, 1999; Pöschl, 2005; Seinfeld and Pandis, 2016). The sources of these particles are diverse, and broadly categorized into natural and anthropogenic origin. Natural sources encompass desert dust storms, volcanic eruptions, biogenic emissions from vegetation, natural wildfires, and sea spray from oceans. On the other hand, anthropogenic sources include industrial activities, transportation emissions, as well as agricultural and livestock activities. Figure 1.1 illustrates some common sources of aerosols.

Figure 1.1 Diverse sources of aerosols from natural and anthropogenic origins. Images sourced from online databases (Credit: Chrissy Sexton, Peter Hartree, CC0 Public Domain, Julia Petrenko/Greenpeace, Tony Hisgett, Water Europe, NYMag, Jonathan Billinger.)

During their stay in the atmosphere, aerosols can have significant impacts on human health, environment and climate change, as illustrated in Figure 1.2. Exposure to certain aerosols can have detrimental health effects, including respiratory and cardiovascular diseases (Arfin et al., 2023). For instance, $PM_{2.5}$ which refers to particulate matter smaller than 2.5 μm in diameter, is known to penetrate deeply into the respiratory tract, leading to asthma, lung cancer, and reduction in lung function (Mannucci and Franchini, 2017; Bové et al., 2019; Kelly and Fussell, 2015). In 2019, the World Health Organization (WHO) assessed that around 6.7 million premature fatalities were linked to both outdoor and indoor air pollution, specifically from $PM_{2.5}$. Out of these, 4.2 million fatalities were directly associated with exposure to outdoor air pollution (World Health Organization, 2023).

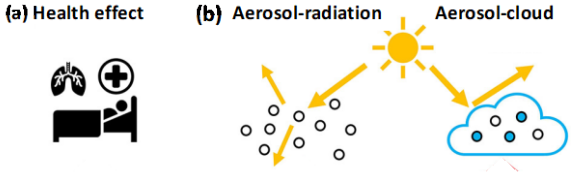

Figure 1.2 Schematic representation of the impacts of aerosols on human health and climate. Figure adapted from Jo et al. (2023)

On the other hand, aerosols also have effects on the environment and climate, as illustrated in Figure 1.2(b). Aerosols can alter the radiative balance of the earth through scattering and absorption of solar radiation, a process referred to as aerosol-radiation interaction (ARI) (IPCC, 2013a). Non-absorbing aerosols, such as sulfate and nitrate aerosols, reflect solar radiation, leading to a cooling of the climate, whereas others, like black carbon and brown carbon, also absorb solar radiation, leading to a warming effect on climate (Lohmann and Feichter, 2005b; Ramanathan et al., 2001). Additionally, aerosols can act as cloud condensation nuclei (CCN), facilitating cloud formation. Specifically, anthropogenic aerosols significantly alter cloud properties through the enhancement of cloud droplet concentration. The increase in CCN concentration leads to smaller, more numerous cloud droplets, which increases cloud albedo and can extend cloud lifetimes and increase cloud cover (Twomey, 1977a; Boucher et al., 2013). This is known as aerosol-cloud interaction (ACI) and generally has a cooling effect on climate, although the magnitude is currently very uncertain. The changes in Effective Radiative Forcing (ERF) from 1750 to 2019 as summarized in the Sixth Assessment Report by the Intergovernmental Panel on Climate Change (IPCC, 2013a), are shown in Figure 1.3. ERF is defined as “change in the net downward radiative flux within the top of the atmosphere (TOA) after allowing atmospheric conditions to adjust (e.g. temperature, water vapor, and clouds), but with surface temperatures or some of the surface conditions remaining unchanged from their initial states” (Myhre et al., 2013). It is used to assess the impact of different factors such as greenhouse gases, aerosols, and land use changes on the earth's climate system (Andrews et al., 2021; J. Smith et al., 2020). The IPCC report highlights that aerosols induce a negative ERF through both ARI and ACI. Specifically, the ERF value from ARI is -0.22 W m^{-2}, with a range of -0.47 to 0.04 W m^{-2}, while ACI contributes to an ERF of -0.84, ranging from -1.45 to -0.25 (IPCC, 2021). These negative values indicate the significant role that aerosols play in mitigating global warming.

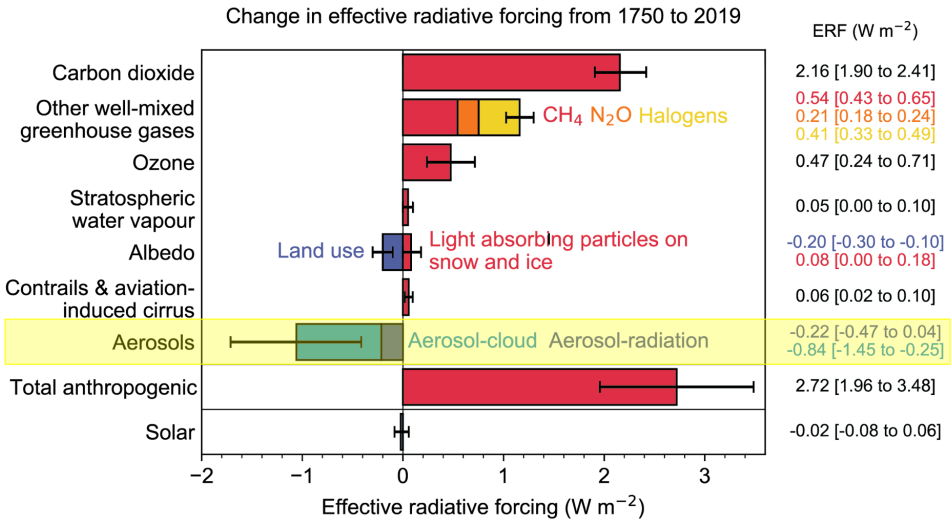

Figure 1.3 Changes in Effective Radiative Forcing (ERF) from 1750 to 2019 are attributed to various factors. This figure highlights the cooling impact of aerosols on the climate, as evidenced by their negative ERF values (marked with a light-yellow background). Figure obtained from the IPCC 6th report (Intergovernmental Panel on Climate Change, 2021).

1.2 Aerosol size distribution

The study of particle size is crucial because both health effects and climate effects of aerosols strongly depend on particle size. The particle size distribution (PSD) of atmospheric aerosols is highly variable, spanning several orders of magnitude from a few nanometers to tens of micrometers in diameter, as shown in Figure 1.4 (Buseck and Adachi, 2008). The PSD can be presented in different ways, such as number size distribution (black solid curve in Figure 1.4), surface area size distribution (orange area in Figure 1.4), volume size distribution, and mass size distribution (yellow area in Figure 1.4). Typically, the number size distribution is obtained through direct measurement and is therefore widely used. The PSD of aerosols in the atmosphere typically follows a log-normal distribution (black dashed lines in Figure 1.4), given as:

$$\mathrm{f(d)} = \frac{1}{d\sigma\sqrt{2\pi}} \exp\left(-\frac{(lnd - ln\mu)^2}{2\ln^2\sigma}\right), \tag{1.1}$$

where d is the particle diameter (nm), μ is the geometric mean diameter, and σ is the geometric standard deviation.

The PSD can be divided into several main modes based on particle diameter: nucleation mode (approximately 1 nm to 10 nm), mainly consisting of newly formed particles; Aitken mode (ranging from 10 nm to 100 nm) with emissions from combustion as an important source; and accumulation mode (from 100 nm to 2.5 μm), where particles have grown from smaller

sizes by condensation and coagulation or are to a smaller extent emitted directly from combustion; as well as coarse mode (exceeding 2.5 µm), primarily composed of dust, sea salt, biological material (e.g. pollen, spores), and volcanic emissions from natural processes. However, in the ambient atmosphere, there is not a strict division, but rather a certain degree of overlap exists between the modes. In general, the shape of the size distribution and the relative abundance of each mode are influenced by multiple factors such as aerosol sources, atmospheric dynamics, and geographic context. For instance, urban settings are likely to exhibit a pronounced Aitken mode, predominantly due to vehicular emissions and industrial activities (Wu and Boor, 2021; Sánchez P. et al., 2021), while remote coastal settings may demonstrate a prominent presence of the coarse mode due to sea salt emissions of breaking ocean waves (Mamali et al., 2018; Sánchez P. et al., 2021).

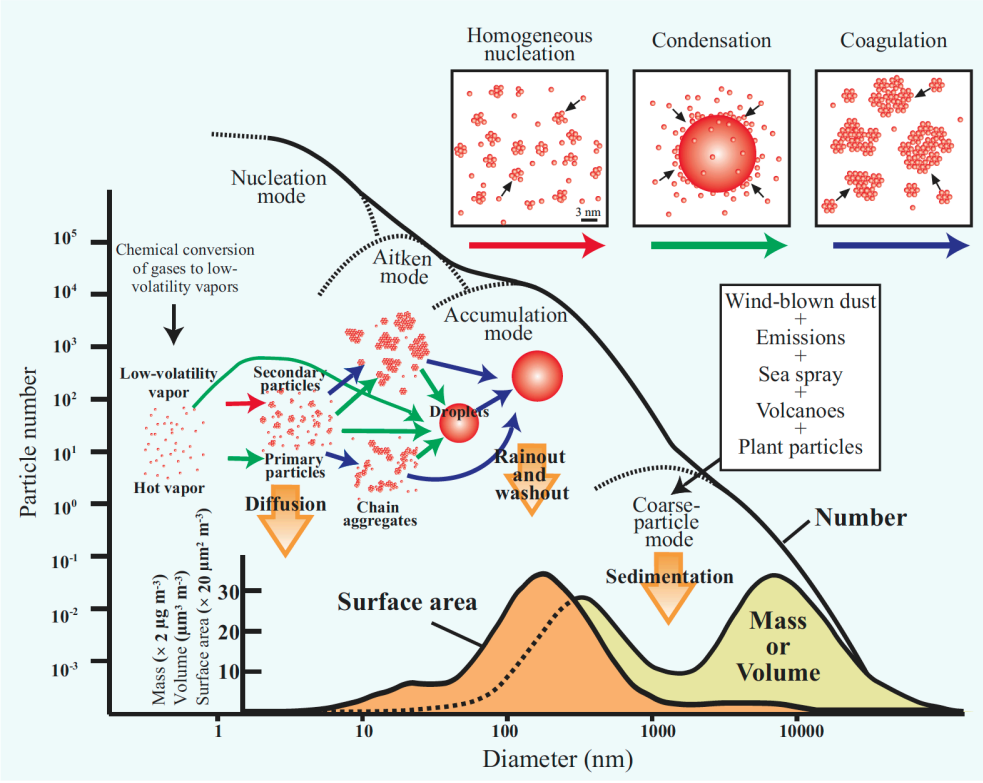

Figure 1.4 Size distribution ranges of different aerosols and their processes and roles in the atmospheric environment (Buseck and Adachi, 2008)

Although the size range of aerosols in the atmosphere is very broad, their number concentration is primarily determined by nucleation and Aitken mode particles, which have diameters less than 100 nm and are commonly referred to as ultrafine particles (UFPs) (Cheung and Chou, 2013; Agudelo-Castañeda et al., 2019; Ridolfo et al., 2024). In addition to the direct emissions, new particle formation (NPF) and subsequent growth significantly

contribute to UFP concentrations. NPF involves complex physicochemical processes, making it challenging to predict UFP concentrations and their environmental and climatic impacts (Brean et al., 2023; Kulmala et al., 2022; Zhao et al., 2024). NPF involves the initial formation of molecular clusters and their subsequent growth into larger particles (Kulmala et al., 2012, 2004; Kulmala and Kerminen, 2008). Typical NPF in the atmosphere starts with the oxidation of precursor gases, such as sulfur dioxide (SO_2), leading to the production of sulfuric acid (H_2SO_4). This is followed by the nucleation of H_2SO_4 (indicated by the red arrow in Figure 1.4), often in the presence of water vapor, resulting in the formation of critical clusters approximately 1-2 nm in diameter. These clusters are stabilized by chemicals such as ammonia (NH_3) and amines (e.g., Dimethylamine, DMA) (Kulmala et al., 2013; McMurry et al., 2005). In addition to H_2SO_4 nucleation, studies have uncovered additional NPF mechanisms. For instance, in northern forest regions with low sulfuric acid pollution, highly oxygenated organic molecules (HOMs) produced from the oxidation of monoterpenes are capable of forming and growing ion clusters (Rose et al., 2018; Bianchi et al., 2019; Kirkby et al., 2016). While in coastal regions, iodic acid (HIO_3) initiated nucleation has been observed (O'Dowd et al., 2002; Sipilä et al., 2016; He et al., 2021). Those newly formed particles or small particles from direct emissions can grow through the condensation of gases, e.g., sulfuric acid or organic vapors (indicated by the green arrow in Figure 1.4) or coagulation with other pre-existing particles (indicated by the blue arrow in Figure 1.4) (Riipinen et al., 2011; Smith et al., 2008; Zhang et al., 2004a). Under supersaturated conditions, water vapor condenses onto particles that reach CCN size, typically larger than 60-100 nm, forming cloud droplets. These droplets then participate in cloud formation and the dynamics of the atmospheric water cycle.

Aerosols can be removed from the atmosphere through various mechanisms, as indicated by the broad orange arrows in Figure 1.4. Diffusion involves the random movement of particles from higher concentration regions to lower concentration regions, removing smaller particles as they diffuse to surfaces and larger particles. Particles that can act as CCN eventually form rain that falls to the ground, and aerosols are also washed out by collision with falling raindrops. Larger particles are normally removed from the atmosphere through sedimentation due to gravitational forces.

In summary, analyzing the PSD offers critical insights into the aerosol sources, growth and removal mechanisms. Figure 1.4 content highlights the complexity of aerosol sources, formation mechanisms, and removal processes across different particle size ranges. This complexity underscores the necessity for region-specific studies to accurately assess their atmospheric impacts and to develop effective strategies to mitigate the environmental and climatic effects of aerosols.

1.3 Aerosol chemical composition

The chemical composition of aerosols also varies significantly depending on their sources. As illustrated in Figure 1.5, aerosols can be produced via two primary pathways: Primary aerosols, which are emitted directly into the atmosphere from their sources. These particles include primary organic aerosols (POA), elemental carbon (EC) or black carbon (BC), mineral dust (MD), sea salt (SS), etc. Secondary aerosols, on the other hand, are particles formed in the atmosphere through chemical reactions. Secondary aerosols mainly include secondary organic aerosols (SOA) and secondary inorganic aerosols (SIA). Different chemical compositions have varying influences on the environment and climate.

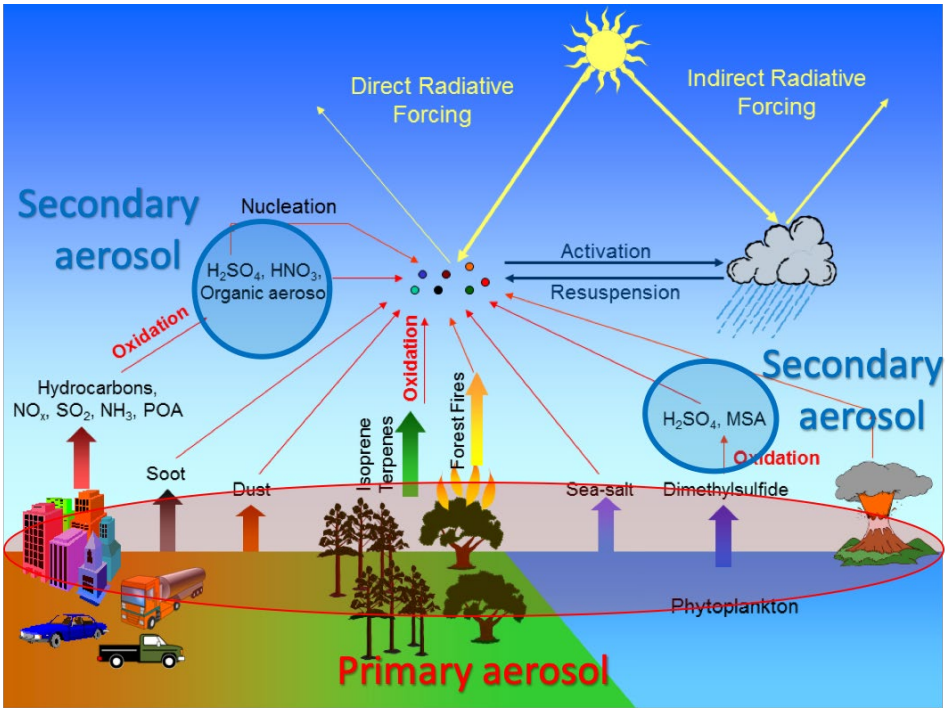

Figure 1.5 Schematic of difference sources and chemical composition of aerosols, and their effects on atmospheric radiation (Adapted from the figure provided by Brookhaven National Laboratory).

Organic aerosols (OA) constitute 20-90% of $PM_{2.5}$ mass concentrations (Kanakidou et al., 2005). POA is directly emitted into the atmosphere from various sources. It consists of a complex mixture of different organic compounds such as hydrocarbons, polycyclic aromatic hydrocarbons (PAHs), and other carbonaceous molecules. SOA accounts for 30-90% of the total OA and forms in the atmosphere through the oxidation of volatile organic compounds (VOCs) (Jimenez et al., 2009; Zhao et al., 2016). These VOCs originate from both natural sources, such as vegetation that emits isoprene, monoterpenes, and sesquiterpenes, or marine

phytoplankton that emits dimethyl sulfide (DMS), and from anthropogenic sources such as industrial activities and vehicle emissions that emit benzene, toluene, and xylene. Overall, the chemical composition of OA is highly complex.

EC also referred to as BC, is emitted as a by-product of incomplete combustion from sources like vehicle engines, biomass burning, and industrial processes. It is a strong absorber of sunlight, which not only contributes significantly to atmospheric warming but also accelerates the melting of ice and snow (Flanner et al., 2009; Gustafsson and Ramanathan, 2016). This feature distinguishes EC from most other aerosol components, which typically have a cooling effect on the atmosphere.

SIA originates from chemical reactions involving the oxidation of sulfur dioxides (SO_2) and nitrogen oxides (NOx), ammonia (NH_3). The primary sources of SO_2 and NOx are the combustion of fossil fuels in industrial processes and vehicles, while NH_3 is predominantly emitted from agricultural and livestock activities (Clappier et al., 2021). These gases are oxidized in the atmosphere and converted into inorganic salts such as sulfates (SO_4^{2-}), nitrates (NO_3^-), and ammonium (NH_4^+) (Allen et al., 2019; Squizzato et al., 2013). The high hygroscopicity of inorganic salts makes them likely to act as CCN (Pöhlker et al., 2023), which consequently influences the climate. Furthermore, SIAs are major contributors to nitrogen deposition, acid rain, and haze, posing serious threats to environmental quality and public health (Xie et al., 2023; Allen et al., 2019).

MD often originates from arid regions and desert soils, being lifted into the atmosphere by wind erosion. These particles are composed of elements such as silicon, aluminum, iron, and calcium, and they can be transported over long distances. The ERF for dust is estimated to be -0.2 ± 0.5 W m^{-2} (90% confidence interval), suggesting that dust plays a role in cooling the Earth's climate (Kok et al., 2023). Since the pre-industrial period, there has been an increase in the global dust mass load by approximately 55 ± 30%, highlighting the considerable influence of dust on the Earth's energy budget (Kok et al., 2023).

SS is generated from ocean spray, are predominantly found near coastal areas but can also be transported inland. Since about 75% of the Earth's surface is ocean, SS is the largest natural contributor to primary aerosols (Lewis and Schwartz, 2004). Particularly in the Arctic region, the warming rate is nearly four times the global average. This is partially due to the production of fine SS aerosol by the sublimation of blowing snow, which enhances the longwave emissivity of clouds and has a strong warming effect on the Arctic surface temperature (Gong et al., 2023).

Currently, there are various measurement techniques available to analyze the chemical composition of aerosols. The aerosol mass spectrometer (AMS), equipped with either a quadrupole (Q-AMS) or time-of-flight (TOF-AMS) detector, is the most commonly used instrument for aerosol chemical measurements (Jayne et al., 2000; Drewnick et al., 2005). The quadrupole Aerosol Chemical Speciation Monitor (Q-ACSM) was developed based on the AMS and is widely used due to its advantages of being portable, economical, and

relatively easy to operate (Ng et al., 2011). Subsequently, the TOF-ACSM was introduced, offering better mass resolution and a better detection limit (Fröhlich et al., 2013). Since the advent of TOF-ACSM, it has been continuously improved, particularly in aspects such as aerodynamic lenses, and vaporizers (Fröhlich et al., 2013; Xu et al., 2017; Freney et al., 2019). Therefore, it is crucial to validate and assess the performance of these various instrument configuration in field measurements, which then allows more accurate quantification of the chemical composition of aerosols.

1.4 Aerosol optical properties

The optical properties of aerosol particles significantly influence atmospheric visibility and climate forcing. The ability of aerosols to scatter and absorb light depends on the size, refractive index, and shape of aerosols (Tanaka et al., 1983). The decrease in light intensity as light passes through an aerosol layer is given by the Lambert-Beer law:

$$\frac{I}{I_0} = e^{-\sigma l}, \tag{1.2}$$

where I_0 is the initial intensity of the incident light, I is the light intensity after passing through a material of path length l, and σ is the extinction coefficient, which can be expressed as the sum of scattering and absorption coefficient. The amount and angular distribution of the light scattered by aerosol particles depend strongly on the aerosol size parameter α, defined as $\alpha = 2\pi r / \lambda$, where r is the particle radius and λ is the wavelength of light. Based on the range of the α, there are three main types of atmospheric light scattering (Bohren and Huffman, 1983):

Rayleigh scattering occurs when α is much less than 1 ($\alpha << 1$). This regime is applicable to particles significantly smaller than the wavelength of light.

Mie scattering is relevant for particles with a size parameter approximately equal to 1 ($\alpha \approx 1$). This regime is applicable to particles about the same size as the wavelength of light.

Geometric optical scattering is applicable when the size parameter exceeds 1 ($\alpha >> 1$).

Mie scattering is most relevant for aerosol effects on visibility and climate. It was initially developed to describe the scattering of electromagnetic waves by spherical particles. Mie theory has been extensively adapted for use in the study of atmospheric aerosols. Based on the assumption that aerosol particles are spherical, Mie theory is used to predict the aerosol optical properties based on the particle diameter (d_p) and refractive index (m), as well as the wavelength (λ) of the incident light.

In simple terms, for a given particle diameter d_p, the aerosol scattering coefficient can be expressed as the product of the scattering cross-section and the aerosol number concentration. Here, the scattering cross-section is defined as the product of the particle geometric cross-

section (that is, $\frac{1}{4}\pi {d_p}^2$) and its scattering efficiency (Q_{sca}). For a polydisperse aerosol, the analytical expression for the relevant coefficients is derived by integrating over the particle number size distribution:

$$\sigma_i = \int_0^\infty \frac{1}{4}\pi {d_p}^2 Q_i(d_p, m, \lambda)\mathrm{n}(d_p) dd_p \tag{1.3}$$

where $n(d_p)$ is the number density of particles at diameter d_p, and the subscript i represents the optical parameters, e.g., scattering, absorption, etc. The efficiencies Q_i in the Mie scattering function are given below:

$$Q_{sca} = \frac{2}{\alpha^2}\sum_{n=1}^{n_{max}}(2n+1)(|a_n|^2 + |b_n|^2) \tag{1.4}$$

$$Q_{ext} = \frac{2}{\alpha^2}\sum_{n=1}^{n_{max}}(2n+1)Re\{a_n + b_n\} \tag{1.5}$$

$$Q_{abs} = Q_{ext} - Q_{sca} \tag{1.6}$$

$$Q_{back} = \frac{1}{\alpha^2}\left|\sum_{n=1}^{n_{max}}(2n+1)(-1)^n(a_n - b_n)\right|,^2 \tag{1.7}$$

where n is an integer representing the index of the infinite series, α is the aerosol size parameter mentioned earlier, a_n and b_n are the Mie coefficients. Their calculation is given in B&H, equations 4.88 and 4.89 (Bohren and Huffman, 1983). A discussion of Mie theory is beyond the scope of this introduction. However, extensive literature is available on the derivations of Mie scattering theory, and many computational models are developed to apply these principles in practical scenarios. (Gutiérrez-Reyes et al., 2014; Hinamoto and Fujii, 2021; Sumlin et al., 2018a).

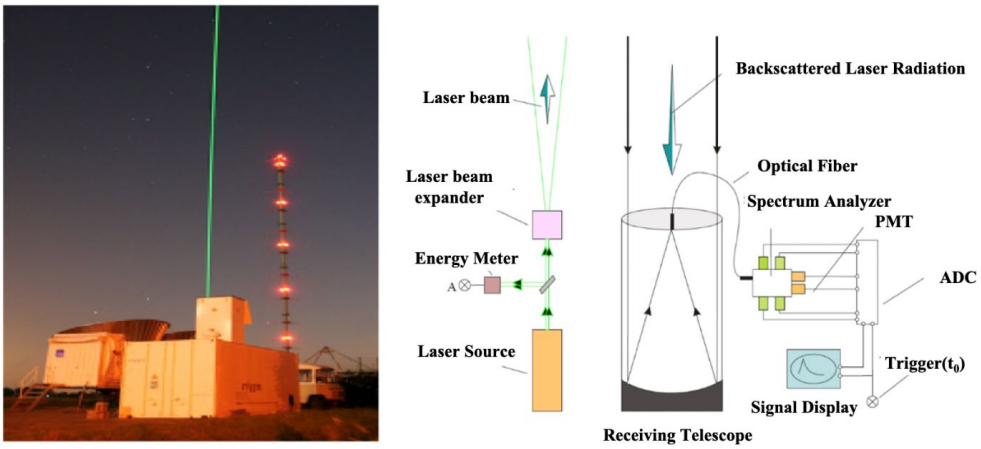

Figure 1.6 The Raman lidar, Caeli, in operation adjacent to the KNMI meteorological tower at Cabauw. Photograph from Apituley et al., (2012). Lidar schematic from the 28th International Laser Radar Conference, Tutorial, 25 June 2017, Bucharest, Romania

In addition to theoretical calculations, the optical properties of aerosols can also be determined through direct measurement techniques. Light detection and ranging (lidar) is one of the technologies extensively employed for this purpose (Ceolato and Berg, 2021; Comerón et al., 2017). Figure 1.6 shows a photo of the Raman lidar used in this study, along with a simple schematic diagram of how the lidar system works. Initially, a laser beam is emitted vertically into the atmosphere. Some of the light is scattered back by interaction with gas molecules and aerosols and captured by a receiving telescope. If the frequency and energy of the backscattered light remain unchanged from those of the incident light, the process is known as elastic scattering. Conversely, if the frequency and energy change, the process is referred to as inelastic scattering or Raman scattering. The backscattered light is transmitted through an optical fiber to a spectrum analyzer, which decomposes the light into its spectral components for detailed analysis. The light signals are then converted into electronic signals by a photomultiplier tube (PMT) and digitized by an analog-to-digital converter (ADC) in a transient analyzer.

Based on Weitkamp (2005a), the lidar equation for the detected signal can be written as:

$$P(R,\lambda) = P_0 \frac{c\tau}{2} A\eta \frac{O(R)}{R^2} \beta(R,\lambda) exp\left[-2\int_0^R \alpha(R,\lambda)\, dr\right] \quad (1.8)$$

The first part, $P_0 \frac{c\tau}{2} A\eta$, is a system factor to describe the instrument performance. The average power of an individual laser pulse is given by P_0, while τ denotes the duration of the pulse, and c is the speed of the light. The area of the primary receiver optics is given by A and the total efficiency of the system is expressed as η.

The second part, $\frac{O(R)}{R^2}$, is a distance (R)-dependent geometric factor, where O(R) represents the overlap function of the laser beam with the receiver-field-of-view (FOV) and R represents

the distance from the lidar system to the target. In an ideal scenario, the scattered light returned from the entire laser beam falls completely within the receiver-FOV, achieving full overlap. However, in reality, issues such as beam divergence beyond the receiver-FOV or imperfect alignment between the emitter and receiver can lead to incomplete overlap or even no overlap at all, resulting in blind zones. Consequently, only optical profiles above a certain height can be accurately recorded (Rosati et al., 2016; Hervo et al., 2016; Wandinger and Ansmann, 2002).

The two parts mentioned above are the experiment setup parameters and can be controlled by the lidar operator.

$\beta(R,\lambda)$ is the lidar backscatter coefficient, which describes how much light is scattered back into the direction of incident light. It is the scattering coefficient value specifically at 180°. $\beta(R,\lambda)$ includes the backscatter coefficients of air molecules and particles. The last remaining unknown value is $\alpha(R,\lambda)$, which is the lidar extinction coefficient, a sum of the scattering coefficients and absorption coefficients of the air molecules and particles. The scattering properties of molecules can be approximately calculated using appropriate standard atmospheric conditions, thereby only the aerosol backscatter coefficient and extinction coefficient need to be determined in the lidar equation (Weitkamp, 2005a).

For a commonly used simple elastic lidar, it is typically assumed that the extinction-to-backscatter ratio (lidar ratio, LR) is a constant value in order to calculate the extinction coefficient from the measured backscatter coefficient. However, in reality, the lidar ratio is influenced by factors such as aerosol size distribution, chemical composition, and relative humidity (Noh et al., 2008; Balis et al., 2004; Lopes et al., 2013; Shin et al., 2018; Dawson et al., 2015; Moise et al., 2015). The introduction of Raman lidar has overcome this limitation by enabling the independent measurement of both the extinction coefficient and the backscatter coefficient. The extinction coefficient is determined from the inelastic (Raman) backscatter signal, whereas the backscatter coefficient is derived from the ratio of the elastic backscatter to the Raman backscatter signal (Ansmann et al., 1992b). However, the Raman lidar signal is significantly influenced by sunlight during the daytime, thus it is more commonly used or performs better at night (Weitkamp, 2005a).

1.5 Field measurements

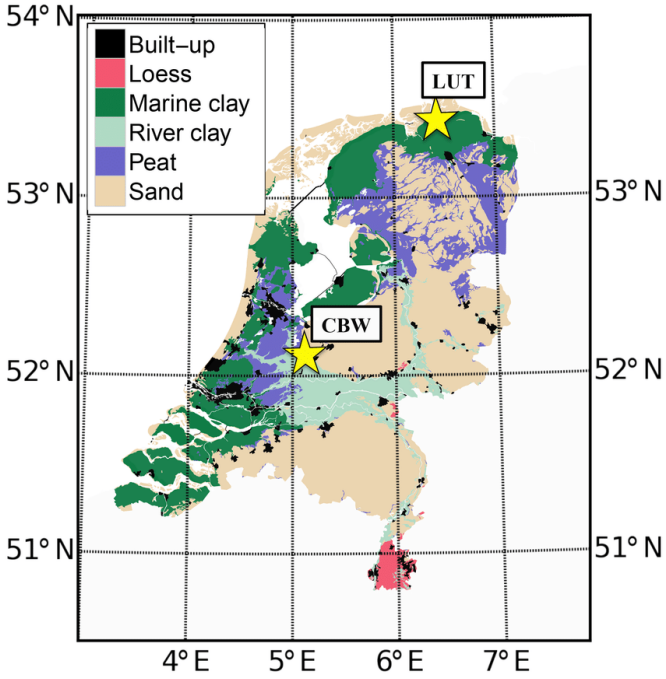

Figure 1.7 Map of research sites (marked with yellow stars) in the Netherlands. CBW represents Cabauw and LUT represents Lutjewad station. Figure from Van Der Laan et al.(2016).

The Ruisdael Observatory (https://ruisdael-observatory.nl/) serves as a fundamental site for meteorological and atmospheric research in the Netherlands. The objective of the Ruisdael Observatory is to execute extensive and precise observations of the atmospheric conditions in the Netherlands, thereby establishing itself as a leading site for atmospheric sciences both in Europe and globally. Figure 1.7 shows a map of the two research sites (Cabauw and Lutjewad) in the Netherlands.

The Cabauw[1] (51.97° N, 4.93° E) station is the principal, most comprehensive, and one of the first established observation stations within the Ruisdael Observatory. It is located in the western part of the Netherlands, at an elevation below 0.7 meters. Although primarily situated in a rural setting, the atmosphere and environment of Cabauw are also affected by adjacent urban centers, notably Utrecht and Rotterdam. As shown in Figure 1.8, the site features a 213-meter measurement tower equipped with meteorological sensors at 2, 10, 20, 40, 80, 140, and 200 meters. Cabauw is equipped with in-situ measurement devices for long-term aerosol monitoring, including an Aerosol Chemical Speciation Monitor (ACSM), a Multi-Angle Absorption Photometer (MAAP), a Scanning Mobility Particle Sizer (SMPS), an

[1] https://ruisdael-observatory.nl/cabauw/

Aerodynamic Particle Sizer (APS), a Cloud Condensation Nuclei Counter (CCNC), and an integrating Nephelometer. Additionally, it employs remote sensing instruments, such as lidar, ceilometer, and radiometer to observe the vertical distribution of aerosols and meteorological parameters, thus providing comprehensive aerosol information.

Figure 1.8 Cabauw research site: the left image shows the Cabauw tower and its surrounding environment, while the right image shows the ground-based in situ instruments room. Photos were taken by the author of this dissertation.

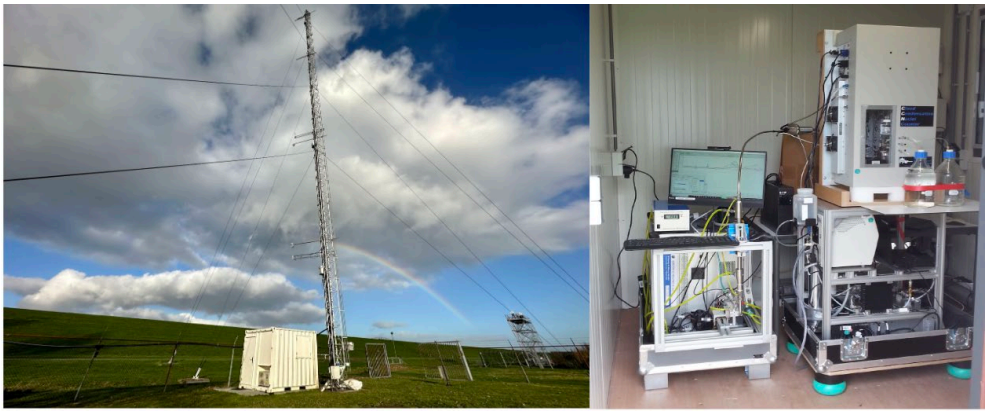

Figure 1.9 Lutjewad research site: the left image shows the Lutjewad tower and its surrounding environment, while the right image shows the ground-based in situ instruments room. Photos were taken by the author of this dissertation.

The Lutjewad[2] (53.24° N, 6.21° E) station, the coastal site within the Ruisdael Observatory, is located on the northern coastline, directly adjoining the Wadden Sea dike as shown in Figure 1.9. It primarily monitors clean background air from the North Sea and continental air pollution carried seawards by southerly winds. Historically, Lutjewad has focused on

[2] https://ruisdael-observatory.nl/lutjewad/

greenhouse gases and their isotopic composition. As a site of the Ruisdael network, it has been expanded to include aerosol observations since 2021. The site features a 60-meter tower and an array of ground-based and remote sensing measurements, such as ACSM, SMPS, CCNC, a disdrometer, a radiometer, and a cloud radar. This aerosol observation station is important for the long-term study of aerosol-cloud interactions.

In summary, Cabauw and Lutjewad are important aerosol stations within the Ruisdael Observatory. This study focuses on both intensive field campaign measurements and long-term observational data from these sites, aiming to provide insights into atmospheric aerosol physical and chemical properties in the Netherlands.

1.6 Objectives and outline of this thesis

This thesis focuses on field observations of aerosols in the Netherlands. The subsequent chapters are outlined briefly as follows: Chapter 2 focuses on the evaluation of the in-situ measurement instruments for aerosols used during field campaigns to ensure the reliability of the measurement results. Chapter 3 develops a model to predict vertical profiles of aerosol optical properties based on the measurement data from the previous chapter, aiming to bridge the gap between in-situ measurements and lidar observations. Chapter 4 switches from the campaign perspective to long-term observation, to investigate new particle formation in different regions of the Netherlands. Chapter 5 provides a discussion and conclusion for the whole thesis.

Chapter 2: Evaluation of TOF-ACSM equipped with $PM_{2.5}$ aerodynamic lens and capture vaporizer

As mentioned, the TOF-ACSM has been widely employed for long-term observation of aerosol chemical composition. However, one major limitation previously encountered was the low transmission efficiency of larger particles, particularly those exceeding 600 nm, due to the low operating pressure of the standard lens system. Additionally, the standard vaporizer, with its inverted cone structure and porous tungsten surface, causes particle bounce instead of vaporizing, thereby reducing collection efficiency. To address these issues, the $PM_{2.5}$ aerodynamic lens and capture vaporizer were introduced successively in 2017 to TOF-ACSM. However, there is still a lack of a comprehensive assessment of this updated configuration in field observations. In chapter 2, we evaluate the capabilities of the TOF-ACSM CV-$PM_{2.5}$ lens by performing a series of comprehensive cross-comparisons between real-time online measurements and offline filter analysis.

We aim to determine whether the new configuration enhances measurement accuracy in field observations and if it can achieve the 30% accuracy level initially specified by the manufacturer. Additionally, we also want to validate its capability for accurately quantifying the mass concentrations of aerosol chemical composition, with a particular focus on $PM_{1.0}$ and $PM_{2.5}$ particles.

Chapter 3: Aerosol optical profile modeling and comparison with Raman lidar

Lidar measurements have become an important tool to study optical properties and their vertical distributions. However, most lidar systems that are operationally used, depend on assumptions of the lidar ratio to derive the aerosol extinction coefficient. Raman lidar systems can retrieve the lidar ratio, but only at higher altitudes and only in the evening/night. In addition, the high cost of lidar techniques also poses challenges to their widespread applications. Therefore, we build a model to predict aerosol optical properties based on routine ground-based aerosol measurements such as chemical composition and size distribution, as well as the readily available weather forecast meteorological data.

In chapter 3, we want to explore, if routine ground-based measurements of aerosol properties can be used to predict the vertical distribution of optical properties, and how comparable these predicted profiles are to Raman lidar retrievals. Furthermore, we aim to understand whether the calculated optical properties from ground measurements can be used to bridge the gap with lidar measurements at higher altitudes.

Chapter 4: Particle size distribution at rural and coastal sites in the Netherlands.

The size of aerosol particles is crucial because it determines their behavior in the atmosphere, including their transport, deposition, and impact on health and climate. The existing studies addressing aerosol PSD in the Netherlands are either short-term or outdated. Consequently, there is a pressing need to examine the characteristics of PSD under the influence of current emission reduction policies. For this purpose, we investigate two years of aerosol observation data from two representative sites in the Netherlands: one from a more polluted regional background site and the other from a remote coastal site.

The objective of Chapter 4 is to understand the characteristics of PSD, including number concentration, sources, and contributions, as well as the temporal trends, across different environments in the Netherlands. The focus of the study is to identify the primary sources of UFPs and the main drivers of NPF, as these are the major contributors to particle number concentrations. We also seek to understand how the current NPF compares to the historical record for the region. Ultimately, by comparing the aerosol and meteorological characteristics between the two locations, the study aims to elucidate the regional and local impacts on PSD.